Underclad Cracks Growth Under Fatigue Loading in Stainless Steel Cladding

J.L. Bernard, F. Bodson, A. Doule, G. Slama
FRAMATOME,
Tour Fiat, F-92084 Paris la Défense Cedex 16, France

M. Bramat, J.P. Doucet, F. Maltrud
Institut de Soudure,
32 Bd. de la Chapelle, F-76880 Paris Cedex 18, France

ABSTRACT

Hydrogen induced cracks have been found in HAZ of pressurized water reactor vessel nozzles under stainless steel cladding. Fatigue tests were performed to collect a large amount of data on the possible propagation of this type of flaws.

Tests were conducted in two steps. The aim of the first step was to set up the experimental equipment and to devise an adequate method for following cracks during fatigue loading. Clad plates with electroerosion machined slots were used for this purpose. The second step was then undertaken with material taken out of an actual nozzle containing hydrogen induced cracks in the HAZ under stainless steel cladding or flaws simulated by electroerosion machined slots.

The test loadings were comparable to in service loadings of the nozzles. Special attention was taken to get representative R ratios ($\frac{\sigma \text{ min.}}{\sigma \text{ max.}}$). Again for the sake of representativity, the tests were performed at 300°C (In service temperature) and the hydrostest was simulated.

The main results are :

- It was possible to follow the whole failure process by combining non destructive examinations during fatigue testing and fractographic observations of broken specimens.
- Different striation patterns, before and after air has penetrated the actual embedded cracks wereobserved.
- Numerical simulation of fatigue crack growth of actual or simulated defects were consistent with experimental data, provided mainly that defect shape, effect of R ratio and of environment were taken into account.

1. INTRODUCTION

Hydrogen induced cracks have been found in the H.A.Z. under stainless steel cladding of pressurized water reactor nozzles. To precise in-service behaviour of such cracks under cyclic loading, fatigue tests have been performed on mock-ups extracted from a nozzle and containing actual hydrogen induced embedded cracks or machined artificial defects in order to precise the following points.

i) Is there an initiation time necessary before an hydrogen induced crack begins to grow ?

ii) How will it propagate in both materials (stainless steel cladding and A 508 Cl 3) ?

iii) How will the shape of the crack change during cyclic loading ?

iiii) Is the absence of either air or agressive medium in cracks reduce the crack growth rate ?

Answering these questions will allow to give estimation of the margins taken in the safety analysis. The experimentation was performed in two steps. The first step was to set up the experimental equipment and to devise the best method for following cracks during fatigue loading of the mock-ups. Cladded plates with electro-erosion machined slots were used for this purpose. The second step was then undertaken with material taken out of an actual nozzle containing hydrogen induced cracks or machined slots in the H.A.Z. under stainless steel cladding.

2. EXPERIMENTAL METHODOLOGY

2.1. Material

The mock-ups tested were taken out of an actual nozzle in A 508 Cl3 containing hydrogen induced cracks in the H.A.Z. under a three layer cladding 309 L/308 L. Chemical and mechanical characteristics of the materials are given in TABLES I and II.

2.2. Test machine and specimens

Tests have been achieved at the "INSTITUT DE SOUDURE" on a 1000 kN servo hydraulic testing machine at the frequency of 0.5 Hz. Tests were performed at room temperature and 300°C In this last case a resistance heating furnace was used. Temperature was maintained constant ($\pm$ 5°C) on the test zone ($\sim$100 mm). Mock-up geometry is given in (Figures 1 a-1b). The central part has been extracted from an actual nozzle with a 309 L/308 L three layer cladding. The heads were welded on this part. Two types of specimens have been used.

1) Specimens with embedded hydrogen induced cracks in the H.A.Z.
2) Specimens with through thickness underclad cracks simulated by electro-erosion machined slots. The machined slots were rectangular with a width of 0.3 mm.

2.3. Methodologies used to follow the crack propagation during fatigue testing.

X ray examination has been used to follow the evolution of embedded hydrogen induced cracks. Special care was taken to localize the X ray source in the plane of the crack and to avoid diffraction by using Pb screens. The X ray source parameters were 285 kV, 10 mA, t = 3 mn, d = 800 mm, front screen 0.05, middle screen 2 x 0.05, back screen 0.05mm.

A travelling microscope (x 30), mounted on a micrometer, was used to follow the evolution of through thickness artificial cracks. Accurate measurements were also done by using replica technic on the cracks.

Beach marks which appears when test is interrupted, were also used to measure the evolution of cracks during fatigue loading.

2.4. Stress an strain measurements

Stress measurements were done by using the load-cell of the testing device. Strain measurements, during testing, were done by using heat resistive strain gages located :
1) On the cladding surronding the cracks and 2) on the opposite face in A 508 C13 base metal under the crack (points 1 and 2 of Figure 2).

The simulation of cold hydrotest (first transcient) was done by imposing a deformation measured by a supplementary strain gage located on the base metal in the vicinity of the crack, just below the cladding (point 3 of figure 2).

2.5. Tests parameters

Before starting the fatigue testing a simulation of the cold hydro test transcient has been applied. This simulation consists in imposing a strain corresponding to an elastic stress ($\sigma = E \times \varepsilon$) equal to 500 MPa.

The tests reported in the present paper consist :

1 - in the simulation of the load follow (15 %-100 %) transient performed at 300°C ; The specimens tested had artificial cracks.

2 - in the simulation of the heat up/cold down transcients performed at 300°C on specimens with actual embedded cracks.

3. RESULTS OF TESTS - DISCUSSION

3.1. Initiation of the fatigue crack

An important feature of the hydrogen induced crack behaviour is that these cracks do not grow immediatly. A period extending between $\frac{Nf}{4}$ and $\frac{Nf}{3}$ (where Nf is the number of cycles to complete failure) is necessary before growth begins. This result has been deduced :

1 - from accurate radiographic examination during interruption of tests at regular intervals and,

2 - from beach marks resulting from interruptions of tests.(Beach marks were observed both with optical microscope and SEM).

Photograph of Figure 3 shows the surface fracture of a specimen broken by tension at 550.000 cycles after a growth was detected by X ray at 515 000 cycles. Successive interruptions of test for X ray examination performed before, produced beach marks which are clearly noticeable. From these marks it was concluded that initiation of a fatigue crack occured for this specimen between 439 000 and 455 000 cycles. Figure 4 shows a typical representation of the evolution of crack length during cycling. An evolution appears only after a period of about $\frac{Nf}{3}$. For all tests a good agreement (15-20%) was found between the starting of the crack growth detected by radiographic examination and the apparition of the beach marks on the surface fracture.

3.2. Fatigue crack geometry

The initial embedded crack geometries can be represented by ellipses with $\frac{a}{c} \simeq \frac{1}{5}$ (typical). It can be observed on figure 5 that the geometry of the elliptical crack changes towards a circular shape.
Some crack deviations occurs during testing. The fracture surface shown in Figure 6 gives an example of such a case. Metallographic study revealed that the deviation, in this case, was due to the presence of segregated area harder than the matrix. This shows that such a segregated area is not a weak zone in fatigue crack growth.

3.3. Environment effects

Hydrogen induced inderclad cracks which are primitively embedded were tested. A particular feature to be noted is that fracture surface aspect changes after the crack has reached the free surface of the specimen. Before, the surface fracture is not well defined and it looks like fractures obtained in vaccuum or inert environment [1 - 2 - 3]. Afterwards, clearly defined fatigue striation immediately appears. These two aspects are shown in Figure 7. Analysis of results (see § 3.4.) points out the different behaviours of crack propagations between actual embedded cracks without external contact and artificial through thickness cracks in contact with air at 300°C.

3.4. Results and analysis of crack propagation tests

Typical evolutions of crack lenghts (or projected crack length when deviation occured) as a function of elapsed cycles, are given in figure 8 to 10. These evolutions concern only the fatigue crack propagation after the crack initiation period. In order to analyse these results a "numerical simulation" of the crack growth, begining after the crack initiation period, has been performed. Such simulations provide a basis to estimate the margins taken in the safety analysis.
The procedure was the following :
- For each case, the crack is supposed to be initiated and to propagate both in base metal and stainless steel cladding.
The numerical simulation is performed by using upper bounds and lower bounds of crack growth rate data available for the two materials, the equations used for these curves are given in table III.
- The hypothesis was done that the level of residual stresses was negligible after the simulation of cold hydrotest.
- The calculations presented here have been performed without any correction for the effects of the differential expansions between stainless steel and base metal ; which is consistent with the high value of σ max and resulting accommodation of the stainless steel.
- Stress intensity factors for elliptical cracks (case of embedded actual cracks) and for through thickness artificial cracks have been computed by using the formulation given by TADA in [4.]

Typical experimental and predicted curves are given in figure 8 to 10.

It appears that :

i) Crack growth of through thickness artificial cracks can be correctly described by the model presented above.

ii) Crack growths of actual embedded cracks are over estimated by the use of the model described above.

There are evidences that an environmental effect is present in the case of embedded cracks. The assumption has been done that the fatigue crack growth rate of the stainless steel cladding is significantly reduced in the medium of the actual cracks.
A reduction of a factor of 4 applied on the fatigue crack growth rate laws of the stainless steel cladding has been applied. It can be seen in Figures 11 and 12 that with this hypothesis the crack growths are correctly predicted with the model described above.

4. CONCLUSIONS

An extensive program has been undertaken to study fatigue crack propagation of both artificial through thickness underclad cracks and actual underclad cracks.
Accurate crack growth measurements have been performed during the tests by using radiographic, optical microscopic and S.E.M. examinations.

Special features of crack propagation have been pointed out :

- an initiation period is necessary before the internal cracks propagate like fatigue cracks.
- crack deviations can occur in the presence of C segregated areas.
- there are evidences that the absence of air or agressive medium induces a decrease in crack growth rate when compared with air results.

Fatigue crack growth of both through thickness artificial and actual embedded cracks in mock ups can be correctly predicted by using a model taking mainly into account the crack geometry, the physical and fatigue properties of the A 508 Cl3 base metal and the 309L/308 cladding.

These experimentations allow to refine the knowledge of margins taken in the current safety analysis.

REFERENCES

[1] HUDSON, C.H., SEWARD, S.K., " A literature review and inventory of the effects of environment on the fatigue behavior of metals ", Engineering Fracture mechanics, 1976, Vol. 8.

[2] MAHONEY, M.W., PATON, N.E., " The influence of gas environment on fatigue crack growth rates in types 316 and 321 stainless steels ", Nuclear Technology, Vol.23, Sept. 1974.

[3] JAMES, L.A., Fatigue crack propagation in austenitic stainless steels, Atomic Energy review, 14-1, 1976, pp 37-86.

[4] TADA, H., The stress analysis of cracks handbook ", DEL Research corporation, Hellertown Pennsylvania, 1973.

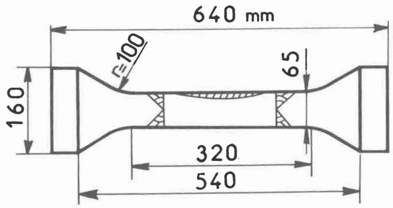

Figure 1a : Specimen geometry

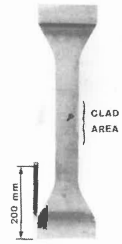

Figure 1b : View of specimen

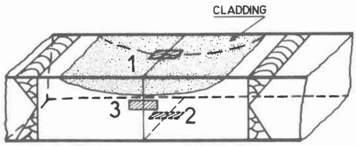

Figure 2 : Detail of central part of the specimen showing strain gages locations

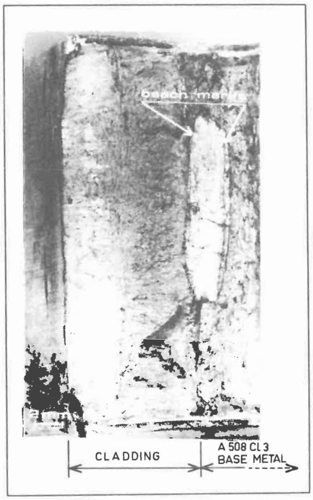

Figure 3 : Fracture surface for a test interrupted at the begining of crack growth (detected by X ray examination) - beach marks appears.

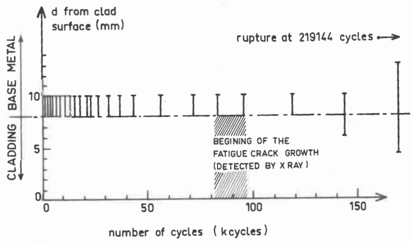

Figure 4 : Evolution of the crack under fatigue loading evaluated by X ray.

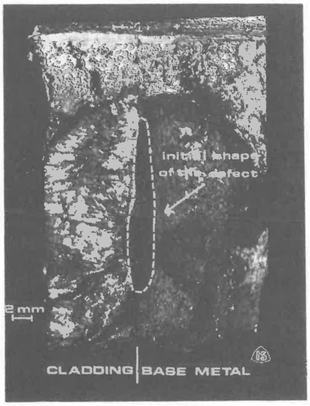

Figure 5 : Evolution of a defect from an elliptical toward a circular shape.

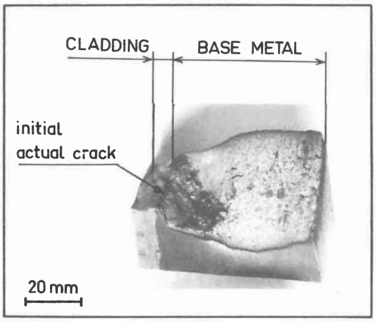

Figure 6 : Deviation of a fatigue crack in A508 Cl 3 base metal.

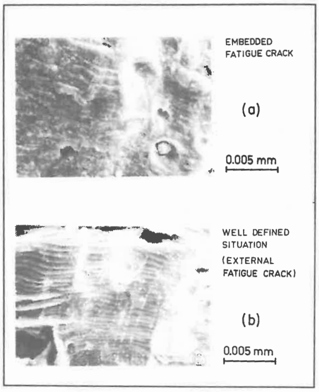

Figure 7 : Difference of fatigue surface aspect before and after the crack has reached the surface of specimen - (a) : embedded fatigue crack - (b) well defined striation (external crack).

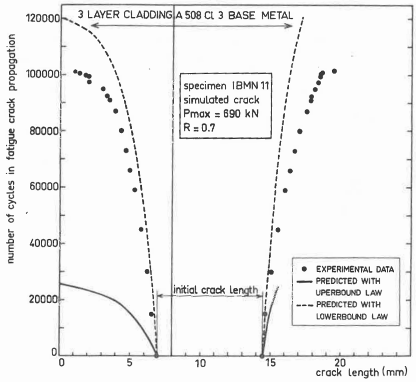

Figure 8 : Simulated defect : evolution of the fatigue crack size as a function of elapsed cycles - comparison with numerical simulation.

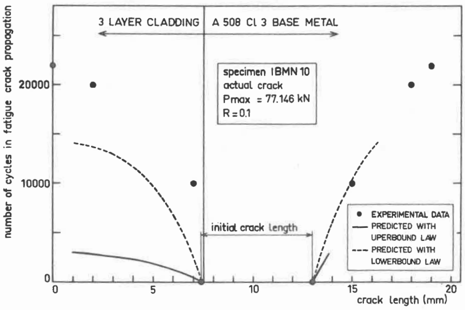

Figure 9 : Actual defect : evolution of the fatigue crack size as a function of elapsed cycles - comparison with numerical simulation.

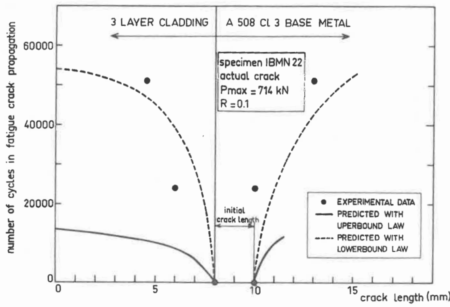

Figure 10 : Actual defect : evolution of the fatigue crack size as a function of elapsed cycles - comparison with numerical simulation.

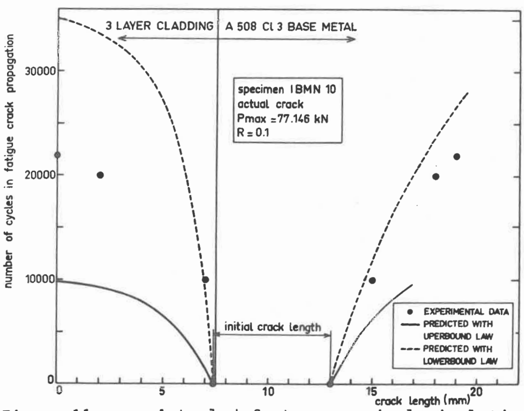

Figure 11 : Actual defect : numerical simulation of fatigue crack growth with the assumption that fatigue crack growth rate in the stainless steel is divided by 4.

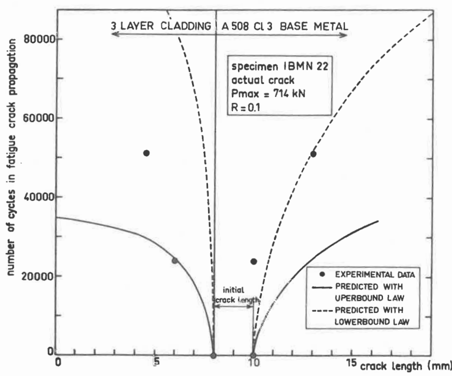

Figure 12 : Actual defect : numerical simulation of fatigue crack growth with the assumption that fatigue crack growth rate in the stainless steel is divided by 4.

TABLE I : Chemical composition of the materials investigated

MATERIAL	C	S	P	Si	Mn	Ni	Cr	Mo	Cu	Co	V
A 508 Cl3 (nozzle)	.16	.006	.009	.280	1.31	.69	.13	.49	.06	.02	.01
(308L) cladding (nozzle)	.023	.011	.015	.830	1.41	10.3	19.97	.096	-	0.25	-

TABLE II : Typical mechanical properties of the materials investigated

MATERIAL	0.2% Yield Strength at R.T. (MPa)	Tensile Strength at R.T. (MPa)	Elongation (5d) at R.T. (%)	Réduction of Area at R.T. (%)	CHARPY V Impact Strength at 0°C (J/cm^2)
A 508 Cl 3	508	634	21.8	67.5	119

TABLE III : Fatigue crack propagation laws used for numerical simulations

Cladding (300°C)	upper bound	$da/dN = 7.5 \times 10^{-10} \left(\frac{\Delta K}{1-\frac{R}{2}}\right)^4$ for all ΔK
	lower bound	$da/dN = 1.3 \times 10^{-10} \left(\frac{\Delta K}{1-\frac{R}{2}}\right)^4$ for all ΔK (mm/cycle) (MPa$\sqrt{m}$)
A 508 Cl 3 base metal 300°C	upper bound	$da/dN = 7.95 \times 10^{-9} \left[K_{max} (1-R)^{0.75}\right]^{2.93}$ for $\Delta K \leq 20$ MPa$\sqrt{m}$ $da/dN = 2.6 \times 10^{-8} (\Delta K)^{2.67}$ for $\Delta K > 20$ MPa$\sqrt{m}$
	lower bound	$da/dN = 3.80 \times 10^{-9} \left[K_{max} (1-R)^{0.75}\right]^{2.93}$ for $\Delta K \leq 20$ MPa$\sqrt{m}$ $da/dN = 1.5 \times 10^{-8} (\Delta K)^{2.67}$ for $\Delta K > 20$ MPa$\sqrt{m}$